

# Near doping-independent pocket area from an antinodal Fermi surface instability in underdoped high temperature superconductors

N. Harrison  
*Los Alamos National Laboratory,  
 MS E536, Los Alamos, New Mexico 87545*

(Dated: February 17, 2022)

Fermi surface models applied to the underdoped cuprates predict the small pocket area to be strongly dependent on doping whereas quantum oscillations in  $\text{YBa}_2\text{Cu}_3\text{O}_{6+x}$  find precisely the opposite to be true – seemingly at odds with the Luttinger volume. We show that such behavior can be explained by an incommensurate antinodal Fermi surface nesting-type instability – further explaining the doping-dependent superstructures seen in cuprates using scanning tunneling microscopy. We develop a Fermi surface reconstruction scheme involving orthogonal density waves in two-dimensions and show that their incommensurate behavior requires momentum-dependent coupling. A co-operative modulation of the charge and bond-strength is therefore suggested.

Identification of the forms of order competing with superconductivity and antiferromagnetism in the high- $T_c$  cuprates remains a considerable experimental challenge [1, 2]. Among possibilities, charge ordering is reported in several experiments within the underdoped regime – namely x-ray diffraction [3], neutron scattering [4], scanning tunneling microscopy (STM) [5] and nuclear quadrupole resonance (NQR) [6] (see Fig. 1a). Yet its extent and relevance are far from understood. It is yet to be established whether such ordering participates in forming the pseudogap [5], whether it is inherently unidirectional as opposed to bidirectional in nature [7], or whether it is caused by a Fermi surface instability [8] as opposed to being a byproduct of spin order [4].

In the light of recent quantum oscillation [9, 10], electrical transport [11] and angle-resolved photoemission spectroscopy (ARPES) [12] studies, several Fermi surface reconstruction models have been invoked in the underdoped cuprates postulating charge (and/or other forms of) ordering [10, 13–15]. A serious problem with *all* proposed models, however, is that they predict the pocket size to be strongly dependent on the hole doping (e.g. dotted and dashed lines in Fig. 1b), whereas experiments on underdoped  $\text{YBa}_2\text{Cu}_3\text{O}_{6+x}$  [16–19] find the pocket area to change remarkably little over a range of hole dopings spanning  $\approx 3\%$  [20] (circles in Fig. 1b).

In this paper, we show that the near doping-independence of the orbit area in underdoped  $\text{YBa}_2\text{Cu}_3\text{O}_{6+x}$  [16, 17, 20] and the increasing charge modulation period seen with hole doping in STM experiments on  $\text{Bi}_{2-y}\text{Pb}_y\text{Sr}_{2-z}\text{La}_z\text{CuO}_{6+x}$  [8] can both be consistently explained by Fermi surface reconstruction resulting from an antinodal Fermi surface nesting-type instability (i.e. at  $[\pm\frac{\pi}{a}, 0]$  and  $[0, \pm\frac{\pi}{b}]$  in Fig. 2a). We present a density wave model in which we mimic incommensurate behavior by considering modulation periods  $\lambda$  corresponding to different rational multiples of the in plane lattice vectors (e.g.  $\lambda = 7/2, 4, 13/3, 9/2, 5, 6$  and 7). On treating scenarios in which the coupling between

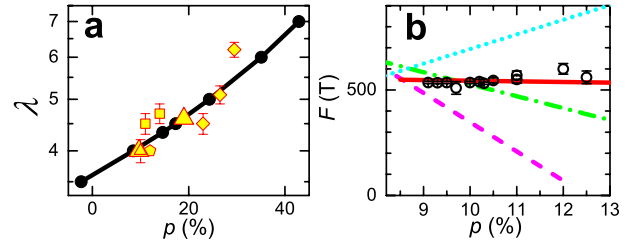


FIG. 1: **a** Charge modulation periods seen using x-rays and NQR in  $\text{YBa}_2\text{Cu}_3\text{O}_{6+x}$  [3, 6] (large triangles), neutrons in  $\text{La}_{0.4}\text{Nd}_{0.4}\text{Sr}_{0.12}\text{CuO}_4$  [4] (pentagon) and STM in  $\text{Bi}_{2-y}\text{Pb}_y\text{Sr}_{2-z}\text{La}_z\text{CuO}_{6+x}$  (diamonds),  $\text{Bi}_2\text{Sr}_2\text{CaCu}_2\text{O}_{8+\delta}$  (squares) and  $\text{Ca}_{2-x}\text{Na}_x\text{CuO}_2\text{Cl}_2$  (small triangle) taken from Ref. [8]. In comparing different materials, we neglect possible differences in  $\varepsilon(\mathbf{k})$  [22]. The line and circles show the  $\rho$  for each  $\lambda$  extracted from the model density-of-states minimum (e.g. Fig. 3b). **b** Measured leading  $\text{YBa}_2\text{Cu}_3\text{O}_{6+x}$  quantum oscillation frequency [16–20] (circles) compared to its strong  $\rho$ -dependence expected in the 4 hole pocket [1] (dotted line), Millis and Norman stripe [13] (dot-dash line) and fixed  $\lambda = 4$  bidirectional charge [15] (dashed line) models, where  $F = (\hbar/2\pi e)A_e$ . The present model (solid line) uniquely yields a weakly  $\rho$ -dependent  $F$  [20].

translated bands is uniform (as in a charge-density wave [13, 15]) or acquires a momentum-dependence (as occurs on incorporating a bond-density wave component [21]), we find that only the latter leads to a single well-defined gap in the electronic density-of-states at weak couplings  $V_{x,y} \ll t_{10}$  (where  $t_{10}$  is the nearest neighbor hopping [22]). We show the latter also to be a necessary prerequisite for incommensurate behavior, in which the electronic structure evolves continuously as a function of  $\lambda$ .

We model Fermi surface reconstruction caused by modulations of general period  $\lambda = n/m$  (in which  $n$  and  $m$  are integers) along the  $a$  and/or  $b$  lattice directions by diagonalizing a Hamiltonian consisting of nested matrices

$$\mathbf{H}_{xy} = \begin{pmatrix} \mathbf{H}_x(0) & V_y \mathbf{I}_n & 0 & \dots & 0 & V_y \mathbf{I}_n \\ V_y \mathbf{I}_n & \mathbf{H}_x(1) & V_y \mathbf{I}_n & \dots & 0 & 0 \\ 0 & V_y \mathbf{I}_n & \mathbf{H}_x(2) & \dots & 0 & 0 \\ \vdots & \vdots & \vdots & \ddots & \vdots & \vdots \\ 0 & 0 & 0 & \dots & \mathbf{H}_x(n'-2) & V_y \mathbf{I}_n \\ V_y \mathbf{I}_n & 0 & 0 & \dots & V_y \mathbf{I}_n & \mathbf{H}_x(n'-1) \end{pmatrix}. \quad (1)$$

Here,  $\mathbf{I}_n$  is an identity matrix of rank  $n$ ,  $n' = n$  for bidirectional order (or  $n' = 1$  for unidirectional order),

$$\mathbf{H}_x(i) = \begin{pmatrix} \varepsilon_{i\mathbf{Q}_y} & V_x & 0 & \dots & 0 & V_x \\ V_x & \varepsilon_{\mathbf{Q}_x+i\mathbf{Q}_y} & V_x & \dots & 0 & 0 \\ 0 & V_x & \varepsilon_{2\mathbf{Q}_x+i\mathbf{Q}_y} & \dots & 0 & 0 \\ \vdots & \vdots & \vdots & \ddots & \vdots & \vdots \\ 0 & 0 & 0 & \dots & \varepsilon_{(n-2)\mathbf{Q}_x+i\mathbf{Q}_y} & V_x \\ V_x & 0 & 0 & \dots & V_x & \varepsilon_{(n-1)\mathbf{Q}_x+i\mathbf{Q}_y} \end{pmatrix}$$

and  $\varepsilon_{j\mathbf{Q}_x+i\mathbf{Q}_y}$  represents the electronic dispersion  $\varepsilon(\mathbf{k})$  [22] subject to translation by multiples of  $\mathbf{Q}_x = [\frac{2\pi}{\lambda a}, 0]$  and  $\mathbf{Q}_y = [0, \frac{2\pi}{\lambda b}]$ .

In the case of a conventional density wave, the normal assumption is for the potentials to uniformly couple all band crossings subject to a relative translation by  $\mathbf{Q}_x$  or  $\mathbf{Q}_y$  such that  $V_x = V_{x,0}$  and  $V_y = V_{y,0}$  are constants in Equation (1). In the case of incommensurate ordering in a two-dimensional lattice, however, the coupling  $V$  has been found to vary depending on the band crossing in question [25, 26]. Such behavior is most apparent in  $R\text{Te}_3$  [25] (owing to its exceptionally large gap), where ARPES finds a momentum-dependent  $V(\mathbf{k})$  that selectively couples portions of the Fermi surface subject to nesting.

While the real-space implications of a momentum-dependent coupling in the chalcogenides has yet to be investigated, in the cuprates it is connected with the possibility of bond-strength or bond-current density wave ordering [21]. We find a simple form of the coupling [27],

$$\begin{aligned} V_x(\mathbf{k}) &= V_{x,0} \frac{1}{1-r} (1 - r \cos bk_y) \\ V_y(\mathbf{k}) &= V_{y,0} \frac{1}{1-r} (1 - r \cos bk_x), \end{aligned} \quad (2)$$

in which  $r$  adds a bond-strength modulation to an otherwise conventional charge-density wave, to prove particularly effective at reducing the electronic density-of states (and consequent free energy) when  $r \approx 1$  [28]. It does so by suppressing  $V(\mathbf{k})$  in the regions of the Brillouin zone where un-nested bands cross [28], which we demonstrate in Fig. 2 by considering the simple case of a unidirectional modulation  $\mathbf{Q}_x = [\frac{2\pi}{\lambda a}, 0]$  [in which  $\lambda = 4$ ,  $n = 4$  and  $n' = 1$  in Equation (1)].

From Figs. 2b and c it is evident that while both uniform ( $r = 0$ ) and strongly momentum-dependent ( $r = 1$ ) forms of  $V_x$  open a gap at  $|k_y| > \frac{\pi}{2b}$ , where the Fermi sur-

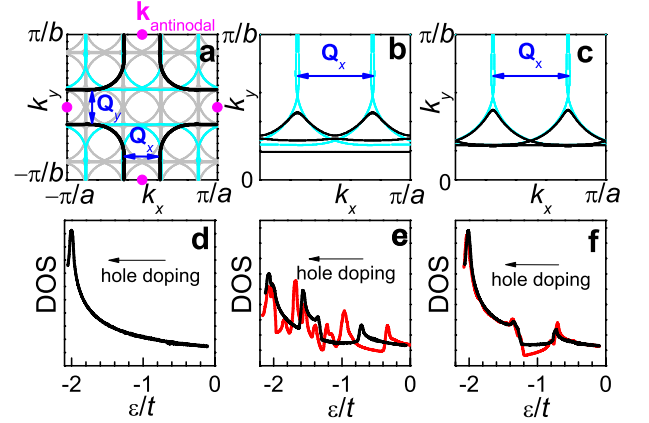


FIG. 2: **a** The unreconstructed Fermi surface at  $p = 8.5\%$  (black) [22] together with itself translated by multiples of  $\mathbf{Q}_x$  (cyan) and multiples of  $\mathbf{Q}_x$  and  $\mathbf{Q}_y$  (grey) for  $\lambda = 4$ . **b** Reconstructed Fermi surface (black) resulting from a unidirectional charge modulation (i.e.  $n' = 1$ ) in which  $V_{x,0} = 0.3t$  and  $r = 0$  in Equation (2), shown for a quadrant of the extended Brillouin zone. **c** Same as (b) but with a momentum-dependent  $V_x$  in which we choose  $r = 1$  [28]. **d** The calculated electronic density-of-states (DOS) for the unreconstructed band [22] exhibiting a van-Hove singularity near  $\varepsilon \approx -2t$ . **e** The calculated DOS (black line) for  $r = 0$  in (b). **f** The calculated DOS (black line) for  $r = 1$  in (c). Red lines in (e) and (f) are the corresponding DOS calculated for concurrent charge modulations along  $a$  and  $b$  (i.e. such that  $n' = n$ ) in which we assume  $V_{x,0} = V_{y,0}$  (by no means a required constraint).

faces are nested by  $\mathbf{Q}_x$ , the latter does so without splitting the open Fermi surfaces at  $k_y \approx \pm \frac{\pi}{4b}$ . The splitting in Fig. 2b occurs concomitantly with an additional gap in the electronic density-of-states at  $\varepsilon \approx -1.8t$  in Fig. 2e and a slightly weaker ordering gap at the Fermi energy ( $\varepsilon_F \approx -t$ ) than in Fig. 2f. A large  $V_x$  at  $|k_y| \approx \frac{\pi}{4b}$  is

therefore energetically unfavorable [28]. The momentum-dependent  $V_x$  (i.e.  $r \approx 1$ ) avoids unfavorable splittings and gaps, leaving the remaining open Fermi surfaces at  $k_y \approx \pm \frac{\pi}{4b}$  amenable to a secondary Fermi surface instability of wavevector  $\mathbf{Q}_y = [0, \frac{2\pi}{\lambda b}]$ , which can further lower the density-of-states (and consequently the electronic energy) by forming a concurrent modulation along  $b$  (red line in Fig. 2f) [where  $n' = n = 4$  in Equation (1) in the case of bidirectional ordering]. By contrast, the splittings caused by a uniform potential (i.e.  $r = 0$ ) mutually disrupt nesting for both  $\mathbf{Q}_x$  and  $\mathbf{Q}_y$  in the case of bidirectional ordering, leading to an energetically unfavorable higher density-of-states consisting of multiple peaks and valleys in the vicinity of the Fermi energy (red line in Fig. 2e).

On extending the bidirectional ordering density-of-states calculation to different periods in Fig. 3, we continue to find a well defined single gap with a broad deep minimum *only* in the case of momentum-dependent coupling (see Fig. 3b), pointing to its continuous evolution with  $\lambda$ . In the case of a uniform coupling (see Fig. 3a), by contrast, the multiple peaks and valleys vary discontinuously with  $\lambda$ .

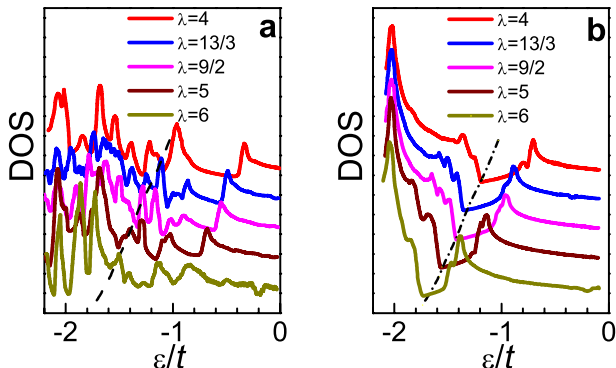


FIG. 3: **a** Electronic density-of-states (DOS) calculated for bidirectional charge modulations with periodicities corresponding to different multiples  $\lambda$  of the  $a$  and  $b$  lattice vectors as indicated, assuming uniform couplings  $V_{x,0} = V_{y,0} = 0.3t$  in which  $r = 0$ . **b** Same as (a) but assuming momentum-dependent couplings in which  $r = 1$  in Equation (2). Curves have been offset for clarity. The dashed line in (b) indicates the minimum in the DOS near to which the Fermi energy is likely to be located.

Thus, by generating a deep wide gap in the density-of-states whose form and location in energy shifts continuously with  $\lambda$ , momentum-dependent coupling provides an incentive for incommensurate behavior in which  $\lambda$  adjusts itself in a continuous fashion so as to lower the electronic energy. Because the electronic energy in an itinerant picture is minimized by having the Fermi energy situated within a broad deep gap in the density-of-states, the  $\lambda$ -dependent gap provides an explanation for the evolution of the periodic structures seen in STM experiments as

a function of doping [8]. The location of the minimum (identified by the dot-dashed line in Fig. 3b) enables us to estimate the hole doping  $p$  at which each period is most likely to be stable (plotted in Fig. 1a). Using these dopings and assuming Luttinger's theorem [29], we calculate the corresponding Fermi surfaces in Fig. 4, whose forms consist of a single electron orbit (located close to the nodes) consistent with experimental observations [15, 30]. Momentum-dependent coupling enables such a pocket to exist for weaker couplings than in ref. [15] and to persist essentially unchanged as a function of doping. Most importantly, the near  $p$ -independent area (solid line in Fig. 1b) reproduces experimental observations (circles).

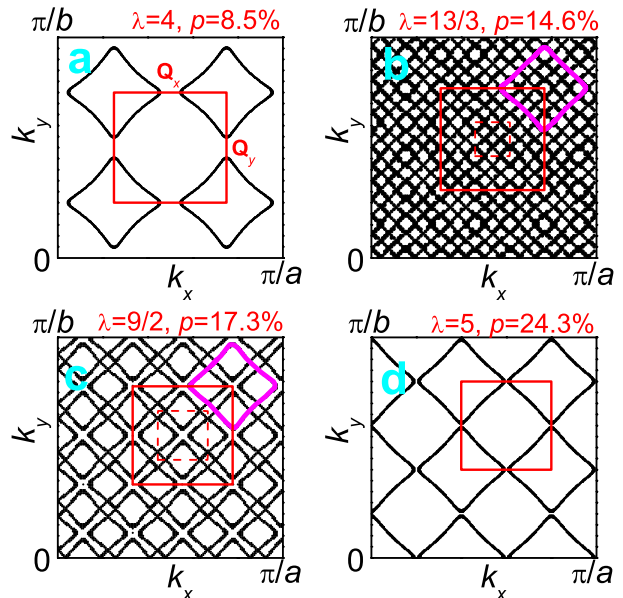


FIG. 4: **a, b, c** and **d** Reconstructed Fermi surface for selected  $\lambda$ 's in Fig. 3b when the Fermi energy is situated at the minimum in the density-of-states, with the corresponding hole doping given. Solid red lines indicate the  $k$ -space area of the  $\lambda a \times \lambda b$  superstructure, while dashed red lines indicate the  $n^2$ -fold reduced Brillouin zone [which coincides with the superstructure in (a) and (d)]. In (b) and (c), a magenta line is used to trace the path of the electron-like orbit that occurs in strong magnetic fields.  $t_{10} \sim 100$  meV [22] produces an effective mass consistent with experiments.

The sub-gaps occurring at the intersections of the electron orbits in Figs. 4b and c are small enough [ $\Delta_{\text{sub}}^2 / BF(\hbar e/m^*)^2 \ll 1$  provided  $V_{x,y} \ll t_{10}$ ] to be completely broken down [31] in magnetic fields of the strength required to see magnetic quantum oscillations [9–11, 16, 17, 30] – giving rise to a single orbit (thick magenta line) in strong magnetic fields. The sub-gaps nevertheless imply the absence of a simple ( $\lambda$ -independent) relationship between the quantum oscillation frequency  $F_e = (\hbar/2\pi e)A_e$  and the frequency  $F_L = \frac{e}{2}F_{\text{BZ}}$  corresponding to the Luttinger hole doping (where  $F_{\text{BZ}} = h/eab$  is the unreconstructed Brillouin zone frequency). Only

when the density-wave is ‘accidentally’ commensurate such that sub-gaps do not occur (e.g.  $\lambda = 4$  or  $5$ ) can adhere to Luttinger’s theorem [29] be easily verified in quantum oscillation experiments. In Fig. 4a, for example,  $F_L = F_\lambda - F_e$  (where  $F_\lambda = F_{BZ}/\lambda^2$  is the  $\lambda a \times \lambda b$  superstructure frequency), while in Fig. 4d it is given by  $F_L = \frac{7}{2}F_\lambda - F_e$ .

Finally, we turn to aspects of momentum-selective density waves that may potentially be reconciled with the unidirectional behavior of charge ordering noted in the cuprates [7]. While closed Fermi surface pockets require charge modulations to occur concurrently along  $a$  and  $b$  lattice directions (in the absence of other orders [15]), the superposition of their ordering gaps in Fig. 2f (red line) implies the absence of a significant energy penalty (or interaction) associated with their coexistence – in contrast to the uniform case in Fig. 2e where such a superposition does not occur. Given the implied independence of the modulations along  $a$  and  $b$ , underlying anisotropies in the electronic structure (such as that caused by the presence of chains in  $\text{YBa}_2\text{Cu}_3\text{O}_{6+x}$  [23]) will likely produce anisotropies in  $V_{x,y,0}$ ,  $\lambda$ ,  $r$  and the onset temperature. In the present simulations, we find a Fermi surface consisting solely of an electron pocket to remain robust against an anisotropy  $V_{x,0}/V_{y,0}$  as large as 4.

In conclusion, we present a model that explains the lack of a detectable doping-dependence of the quantum oscillation frequency in underdoped  $\text{YBa}_2\text{Cu}_3\text{O}_{6+x}$  (i.e. Fig. 1b [20]). By considering rational values of  $\lambda$ , we develop what is in essence an incommensurate model for co-operative charge- and bond-density wave ordering in the cuprates [21, 32] – here driven by a Fermi surface instability at the antinodes. By incorporating a (possibly dominant [28]) bond-density wave component [21], the size of the periodic potential required to produce a single pocket with a small residual density-of-states is greatly reduced (i.e.  $V_{x,y,0} \gtrsim 0.05t_{10}$ ) [28] relative to other models [13–15]. A key strength of the present model is its ability to reconcile doping-dependent quantum oscillations [16–20, 30] with the doping-dependent  $\lambda$  seen in STM and other experiments [3, 6, 8] (i.e. Fig. 1b), the negative Hall and Seebeck coefficients over a broad range of dopings seen in transport [11] and particle-hole symmetry breaking reported at the antinodes in ARPES [2, 12] – all while maintaining compliance with Luttinger’s theorem [29].

The author acknowledges the DOE BES project ‘‘Science at 100 Tesla’’ and useful discussions with Ross McDonald and Arkady Shehter.

- 
- [1] P. A. Lee, N. Nagaosa, X. G. Wen, Rev. Mod. Phys. **78**, 17 (2006).  
 [2] T. Kondo *et al.* Nature **457**, 296 (2009); R.-H. He *et al.* Science **331**, 1571 (2011).

- [3] X. Liu *et al.*, Phys. Rev. B **78**, 134526 (2008).  
 [4] J. M. Tranquada *et al.*, Nature **375**, 561(1995).  
 [5] J. E. Hoffman *et al.* Science **295**, 466 (2002); T. Hanaguri *et al.*, Nature **430**, 1001 (2004).  
 [6] M.-H. Julien, (Aspen Winter Conference, 2011).  
 [7] S. A. Kivelson, Rev. Mod. Phys. **75**, 1201 (2003).  
 [8] W. D. Wise *et al.*, Nature Phys. **4**, 696 (2008).  
 [9] N. Doiron-Leyraud *et al.*, Nature **447**, 565 (2007).  
 [10] E. A. Yelland *et al.*, Phys. Rev. Lett. **100**, 047003 (2008); A. F. Bangura *et al.*, Phys. Rev. Lett. **100**, 047004 (2008).  
 [11] D. LeBoeuf *et al.*, Nature **450**, 533 (2007); F. Laliberté *et al.*, arXiv:1102.0984.  
 [12] M. Hashimoto *et al.* Nature Phys. **6**, 414 (2010).  
 [13] A. J. Millis and M. R. Norman, Phys. Rev. B **76**, 220503 (2007).  
 [14] S. Chakravarty, H. Y. Kee, Proc. Nat. Acad. Sci. USA **105**, 8835 (2008).  
 [15] N. Harrison, S. E. Sebastian, Phys. Rev. Lett. **106**, 226401 (2011).  
 [16] S. E. Sebastian *et al.*, Proc. Nat. Acad. Sci. USA **107**, 6175 (2010).  
 [17] B. Vignolle *et al.*, Comp. Rend. Phys. **12**, 446 (2011).  
 [18] J. Singleton *et al.*, Phys. Rev. Lett. **104**, 86403 (2010).  
 [19] S. E. Sebastian, G. G. Lonzarich, N. Harrison (unpublished).  
 [20] The scatter is related to small number of oscillations at some dopings. Upon close examination, the resistive oscillations of  $\text{YBa}_2\text{Cu}_3\text{O}_{6+x}$  in Refs. [16, 17, 19, 30] are seen to remain essentially in-phase for the range of dopings spanning  $\approx 3\%$ , implying that the same Landau level crosses the Fermi energy at the same field to within  $\Delta B \sim 0.5$  T in all samples regardless of doping. From this we infer  $F$  to change by less than  $(\Delta B/B)F \sim 5$  T (corresponding to  $< 1\%$  change in orbit area  $A_e$ ).  
 [21] C. Nayak, Phys. Rev. B **62**, 4880 (2000).  
 [22] We use  $\varepsilon = \varepsilon_0 + 2t_{10}[\cos ak_x + \cos bk_y] + 2t_{11}[\cos(ak_x + bk_y) + \cos(ak_x - bk_y)] + 2t_{20}[\cos 2ak_x + \cos 2bk_y]$  [23], with  $t_{11}/t_{10} = -0.5$  and  $t_{20}/t_{10} = 0.1$  chosen to reproduce the  $\text{YBa}_2\text{Cu}_3\text{O}_{6+x}$  Fermi surface from recent ARPES [24].  
 [23] O. K. Andersen *et al.*, Phys. Chem. Solids **56**, 1573 (1995).  
 [24] Y. Sassa *et al.*, Phys. Rev. B **83**, 140511 (2011).  
 [25] V. Brouet *et al.*, Phys. Rev. B **77**, 235104 (2008).  
 [26] K. Rossnagel, J. Phys.: Cond. Matt **23**, 1 (2011).  
 [27] The  $k$ -dependent matrix elements in Equation (1) become  $V_x(\mathbf{k} + i\mathbf{Q}_y)$  and  $V_y(\mathbf{k} + j\mathbf{Q}_x)$  where  $i$  and  $j$  refer to the multiples of  $\mathbf{Q}_y$  and  $\mathbf{Q}_x$  by which  $\varepsilon$  is translated. Since the primary function of the  $k$ -dependence is to inhibit splitting of the open sheets in Fig. 2, we neglect the  $k_x$ -dependence of  $V_x$  and the  $k_y$ -dependence of  $V_y$ .  
 [28]  $r$ -dependent calculations reveal the DOS and free energy to be lowest when  $r = 1.35$  (considering  $\lambda = 4$ ) for the Fermi surface considered, implying a dominant bond-density wave component (with  $V_x$  and  $V_y$  exhibiting nodes at  $k_y = \frac{\pi}{b} \pm \frac{|\mathbf{Q}_y|}{2}$  and  $k_x = \frac{\pi}{a} \pm \frac{|\mathbf{Q}_x|}{2}$  respectively).  
 [29] J. M. Luttinger, Phys. Rev. **119**, 1153 (1960).  
 [30] S. E. Sebastian *et al.*, Nature Comm. (in press, 2011).  
 [31] W. M. Lomer, Proceedings of the International Conference on Magnetism (Nottingham, UK, 1964); E. Fawcett, Rev. Mod. Phys. **60**, 209 (1988).  
 [32] S. Sachdev, Rev. Mod. Phys. **75**, 913 (2003).